scientific reports

Check for updates

OPEN

Pedunculopontine-stimulation obstructs hippocampal theta rhythm and halts movement

Jaspreet Kaur[1], Salif A. Komi[1], Oksana Dmytriyeva[2], Grace A. Houser[1], Madelaine C. A. Bonfils[1] & Rune W. Berg[1]✉

While the movement of rodents can be paused by optogenetic stimulation of a brainstem nucleus, the pedunculopontine nucleus (PPN), it is unknown whether this response has a functional purpose. The arrest appears conspicuously similar to fear-induced freezing behavior and could constitute a general halting mechanism for movement without an emotional component. Further, it is unclear to what extent brain activity is affected by the evoked motor arrest. Here, we investigate this phenomenon by engaging a distinct brain activity, the hippocampal theta rhythm. The theta rhythm is prominent during locomotor activity, absent under normal immobile situations, yet present under vigilant states like fear-induced freezing. Specifically, we ask whether the PPN-induced motor arrest has the same effect on the theta rhythm as if the animal would perform a volitional arrest, which results in the disappearance of the theta rhythm, or whether it would cause a continuation of the theta rhythm as would be expected by a fear-induced motor arrest. An alternative hypothesis is that the theta rhythm represents an ongoing intention to move rather than the movement itself. To distinguish between these two possibilities, we recorded the hippocampal brain rhythm before and during movement arrest induced by optogenetic stimulation of the PPN in rats. The PPN-induced motor arrest was associated with a clear obstruction of the ongoing theta activity. The timescale of movement arrest was less than 200 ms, similar to the obstruction of the theta rhythm. Since fear and behavioral freezing are associated with hippocampal theta rhythm, which we did not see during PPN stimulation, we suggest that induced motor arrest occurs without an associated emotional component. Further, our experiments reveal that the theta rhythm during motor activity does not represent an intention, but rather the ongoing sensory-motor state.

Movement arrest, or the temporary cessation of movement, is a common and adaptive aspect of animal and human behavior[1]. It often occurs in response to unexpected events or the sudden appearance of obstacles that demand the immediate suppression of movement[2]. In rodents, for example, freezing behavior is triggered as part of a conditioned pain response or in reaction to looming threats, serving an immediate need for silence and immobility[3]. This movement arrest can also be induced artificially, such as through optogenetic stimulation of specific glutamatergic neurons in the Pedunculopontine Nucleus (PPN), a structure located in the caudal mesencephalon. Studies have observed this PPN-induced arrest in various animals, including mice[4–6], rats[7], and similar activity in cats, which exhibit altered rhythmic and postural motor activity[8,9]. These findings are intriguing because the PPN is part of the midbrain locomotor region (MLR)[10], a brain region typically associated with initiating locomotion rather than suppressing it.

The PPN and the cuneiform nucleus (CnF), another brainstem region, together form the MLR. Both nuclei can evoke locomotion, though with a distinction between slow exploratory behavior and rapid escape responses[5,11,12]. It was recently discovered that CnF contains a subset of cells, which carry D2-receptors, which also have the capacity to pause movement[13], similarly to that seen in PPN. The MLR sends descending fibers to the spinal cord via the reticular formation, activating central pattern generators that produce rhythmic motor sequences through rotational population dynamics[14,15]. Parts of the caudal medulla receive direct input from PPN and project to the spinal cord, and optogenetic activation of cells in the caudal brainstem has similar motor arrests as seen during PPN stimulation[16]. While the capacity of the MLR to activate spinal motor circuits is well established across species[12,13,17–23], the PPN's involvement in modulating behavioral states and controlling sympathetic cardiovascular functions is equally important[24–27]. Thus, the ability of PPN stimulation

[1]Department of Neuroscience, Faculty of Health and Medical Sciences, University of Copenhagen, Blegdamsvej 3, 2200 Copenhagen, Denmark. [2]Novo Nordisk Foundation Center for Basic Metabolic Research, University of Copenhagen, Blegdamsvej 3B, 2200 Copenhagen, Denmark. ✉email: runeb@sund.ku.dk

to induce movement arrest is notable because it reveals that two opposite behaviors-locomotion and movement suppression-can be triggered by stimulating parts of the same nucleus.

This raises several questions regarding the functional role of the PPN in relation to movement and brain state. Could the observed movement arrest be linked to a startle response, or is it associated with a different cognitive state? Interestingly, movement arrest has also been observed during stimulation of neurons in the central amygdala[28,29], suggesting that emotional states may play a role in PPN-induced movement suppression. Additionally, the PPN's connection with the basal ganglia[1,6,30–32] invites speculation about the similarities between this phenomenon and Parkinson's disease symptoms, such as bradykinesia and freezing of gait[33,34]. The PPN's potential involvement in the pathophysiology of Parkinson's disease and its role as a therapeutic target have been suggested in several studies[8,32,35]. However, the diversity of responses to PPN stimulation may depend on both the specific location within the nucleus and the cell types activated[4,7,9,19].

Movement arrest is tightly coupled to the brain's representation of spatial and temporal information. Locomotion must be integrated with event perception[36,37], and activating the PPN has been shown to affect cortical[24,38] and hippocampal activity[39–41]. However, how PPN-induced movement arrest influences the brain's processing of time and space remains unclear. The hippocampus, known for its central role in memory and spatial navigation[36,42], exhibits prominent rhythmic activity known as theta oscillations (6–9 Hz in rodents), especially during movement[43–45] and acceleration[46]. Theta rhythm is often associated with arousal[39] and motor activity[47], but it has primarily been studied in relation to external events. Hence, whether the hippocampal theta rhythm (type 1) represents an ongoing intention to move or the movement itself has been unclear. The internally generated movement arrest induced by PPN stimulation offers a new tool, which is not dependent on external triggers of motor arrest, to address these questions further, since theta rhythm has also been observed during immobile preparedness[48] and heightened emotional states (type 2), such as fear and freezing[49] or panic[50], suggesting that emotions may also be evoked during the PPN-induced arrest.

We formulate three possible effects on the hippocampal theta rhythm when internally inducing motor arrest (Fig. 1). In the first outcome (null hypothesis), we assume higher brain regions cause the theta rhythm, and it represents an ongoing intention to move rather than the movement itself (Fig. 1A). The motor commands are active in a parallel feedforward manner through motor regions in the brainstem and spinal cord. Hence, the motor arrest induced by PPN stimulation does not directly affect the hippocampal formation, and therefore, there will be a sustained continuation of hippocampal theta rhythm. In the second possible outcome (alternative hypothesis), the theta rhythm is contingent on internal monitoring of motor state (efference copy of motor commands, primarily from the brainstem and spinal cord) and sensory feedback (upwards arrows, Fig. 1B). Hence, a PPN-induced motor arrest will also obstruct the theta rhythm (type 1). In the third possible outcome (alternative hypothesis 2), the theta rhythm (type 1) is obstructed. Still, another type of theta rhythm (type 2), which is associated with alertness and fear, is also generated by the PPN stimulation (Fig. 1C). Hence, following the PPN-induced motor arrest, the hippocampal theta rhythm will still be present, but of a different type, representing an alert and sessile state.

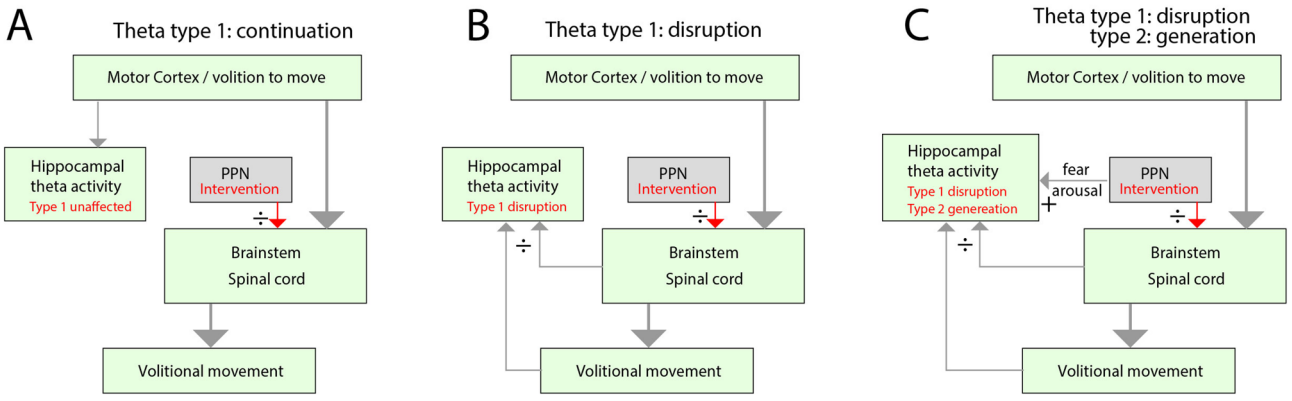

Fig. 1. Possible effects on hippocampal theta rhythm when internally inducing motor arrest by stimulating PPN. (**A**) Null-hypothesis: the motor-related theta activity (type 1) in the hippocampus is generated as a consequence of the intention to move rather than the movement itself. Therefore, theta rhythm continues despite the PPN-induced intervention (red arrows from PPN). (**B**) Alternative hypothesis: The hippocampal theta rhythm is closely tied to the movement via efference copy (from brainstem and spinal cord) and sensory feedback, rather than the intention of movement. Hence, the internally induced motor arrest also disrupts the hippocampal theta rhythm. (**C**) Alternative hypothesis 2: The motor arrest is linked to an alert state, e.g. fear and arousal, and therefore the PPN-stimulation is generating type 2 theta, besides inducing motor arrest and disruption of type 1 theta rhythm. Therefore, hippocampal theta activity will still be present during the PPN stimulation, but of a different type.

Results

The arrest of movement by PPN stimulation

Our first objective was to reproduce the previously reported movement arrest by optogenetic stimulation in the PPN[4,5,7]. The opsin, which induce neural excitation when illuminated with red light (ChrimsonR), was expressed using an AAV virus (AAV9-CamKIIa-ChrimsonR-mScarlet-Kv2.1) injected into the PPN[7] along with the implantation of an optical fiber (Fig. 2A). After expression, the animal was allowed to perform exploratory movements, which were recorded using accelerometers. When optogenetically activating the PPN movement of the animal rapidly came to a halt (Fig. 2B). This is seen as the extinction of the accelerometer measurement coinciding with the PPN stimulation ("PPN stim", blue-shaded regions). When stimulating PPN, the rat would keep its posture at the stimulus onset, which could be seen e.g. while locomoting on a treadmill ("flexed paw pose", Fig. 2C). When the stimulation was stopped, the animal would resume the locomotion (Supplementary Movie 1). This is consistent with the previously reported motor arrest observed in same species[7]. The arrest was quantified in terms of the accelerometer measurement in x, y, and z-directions, which gives an upper limit on the effects on the neural processes. These were triggered at the onset of the stimulus, rectified, and averaged across directions (Fig. 2D). For comparison, the averaged values were integrated at 300 ms after the start of the stimulus ("PPN-stimulation") as well as at 200 ms prior to onset, which served as pre-values ("control"). The movement versus PPN stimulation was compared across stimulus events for the same animal (Fig. 2E) and their median value was compared across animals (Fig. 2F, Supplementary Fig. 1). They all show a significant reduction in movement, in terms of a decrease in accelerometer measurement when the PPN was stimulated.

PPN stimulation and hippocampal theta rhythm

Next, we investigated the effect of PPN stimulation on the hippocampal theta. The theta rhythm was measured using local field potential (LFP) electrodes placed across the first region of the hippocampal circuitry, Cornu Ammonis (CA1), and the dentate gyrus (DG) (Fig. 3A,B). Again, the movement was measured using accelerometers, and the PPN-induced arrest in the movement was seen as the acceleration coming to zero (blue-shaded regions, Fig. 3C). The hippocampal LFP recording exhibited a strong rhythm before PPN stimulation (Fig. 3D), but following the PPN stimulation the rhythm changed. The spectral content changed from having a prominent peak in the theta range (6–9 Hz) to having marginal power in this range (blue band, Fig. 3E). This was also reflected in the integrated spectral content in the theta range, which had a diminishing value after the onset of PPN stimulation (Fig. 3F). In conclusion, PPN stimulation obstructs the ongoing theta rhythm while also halting the movement.

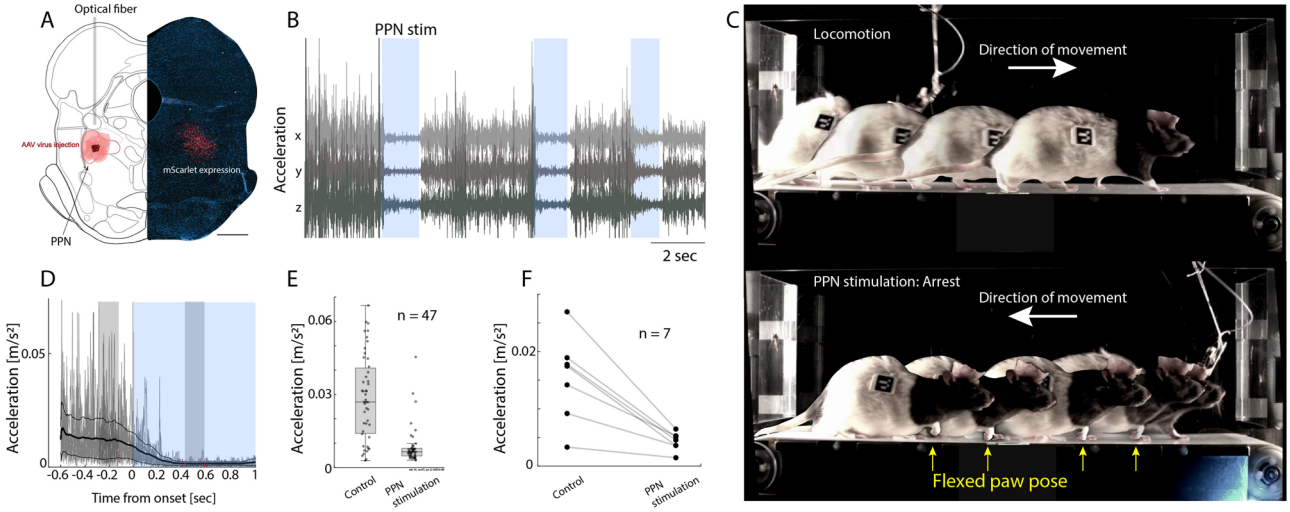

Fig. 2. Optogenetic stimulation of PPN arrests ongoing movement. (**A**) The PPN was targeted in rats using optogenetics via a virus, which expresses an opsin (ChrimsonR) and an implanted optical fiber. A histology section (scale bar= 1000 µm) of the caudal mesencephalon shows the viral reporter (mScarlet) in red and DAPI staining in blue and the corresponding atlas section with injection sites in red. (**B**) Accelerometer readings of movement in 3 directions (anterior–posterior, mediolateral, and dorsoventral), and optical stimulation ("PPN stim", blue regions) induced arrest and eliminated acceleration. (**C**) Chronophotography of rat locomotion on a treadmill. Top: While not stimulating PPN, the rat is moving faster than the belt speed, hence advancing forward. When optically stimulating the PPN, the locomotion is halted (bottom) while keeping its pose). Flexed paw pose is indicated (yellow arrows) while moving backward due to belt movement. (**D**) The stimulation-triggered and averaged rectified accelerometry (black line). The average is integrated across the shaded gray regions across trials as "control" and "PPN stimulation" (**E**). (**F**) The median values across animals (n=7) have a significant decrease when PPN is stimulated. Illustration in (**A**) was adapted with permission[51]. (**C**) Wires from animal (except one) was removed in the picture for simplicity.

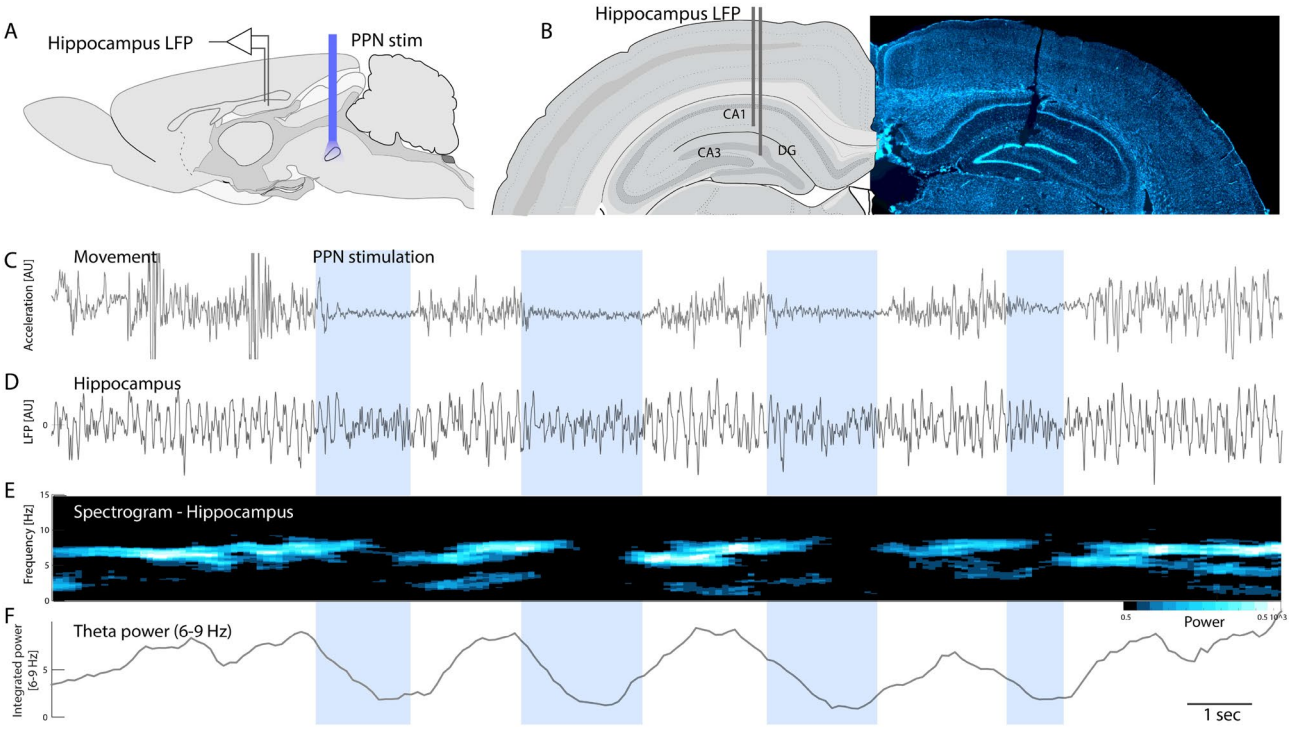

Fig. 3. PPN activation obstructs the hippocampal theta rhythm. (**A**) Sagittal view of the location of the hippocampal LFP electrode and the optical fiber in PPN. (**B**) Coronal histological section showing the LFP electrode across the dentate gyrus and CA3 (dorsal up, fluorescent DAPI stain). (**C**) The arrest of movement of the rat is evident by a drop in acceleration following the onset of PPN stimulation (blue-shaded regions). (**D**) Concurrent LFP activity in the hippocampus with prominent theta rhythm, which evaporates with the PPN stimulation. (**E**) The spectrogram of the hippocampal LFP displays power in theta range which ceases after PPN stimulation. (**F**) The integrated theta band power (6–9 Hz). The histological section in (**B**) is a fluorescent DAPI stain. Illustrations in (A-B) were adapted with permission[51].

Decay of the movement arrest and theta rhythm

What is the delay in movement arrest from the onset of PPN stimulation? The time course of the arrest may provide important clues to the neural mechanisms. Hence, we estimated the course of the movement arrests by fitting an exponential decay, $exp(-t/\tau)$, to the amplitude of the accelerometer data across animals (Fig. 4A). The median value of the time constant, τ, across events and animals ranged from 90 to 200 ms. The mean value across animals was 157 ms (horizontal line, Fig. 4B). These values are larger but comparable to the values of motor arrest in mice[4]. The larger values of motor arrest are likely due to the larger body weight of rats, which is typically twenty times larger than that of mice. Next, we investigated the timescale of movement arrest together with the cessation of the theta rhythm (Fig. 4C). The purpose is to establish a temporal order of the movement arrest compared with the theta rhythm to verify a potential causal relationship. However, due to limitations in the time-frequency resolution, i.e. *the Gabor uncertainty*, the estimation of the change in theta rhythm is difficult to do precisely in time. We used sliding windows of equal size in both measures to mitigate this issue and better compare the temporally well-defined arrest in movement with the less well-defined obstruction of theta rhythm (Fig. 4D). We found that both the accelerometer data and the theta rhythm had decay in activity that was indistinguishable from each other (Fig. 4D–F). The standard deviation of the theta rhythm estimation was larger than the movement arrest, again due to the Gabor uncertainty. This is seen as a larger shaded area (cf. cyan and grey Fig. 4D) and a wider spread of observations in time constants (cyan vs grey, Fig. 4E). Nevertheless, their distributions had a mean that was not significantly different in 3 out of 4 animals (Wilcoxon signed-rank test, $p > 0.05$). We conclude that since the decay in both theta oscillation and the movement is occurring at a similar rate, we cannot establish a causal relationship, only an association between motor arrest and theta obstruction. Nevertheless, the steady-state spectral content of the theta range in the hippocampus was significantly reduced in all animals when the PPN was stimulated (Fig. 4G).

Location of PPN stimulation and cell types

Histology was performed to identify the location of the AAV virus injection, its expression, and optical fiber implantation (Supplementary Figs. 2 and 3). Histological brain sections of rats where a successful movement arrest was observed (Supplementary Fig. 3). The location of the fiber implantation and AAV virus spread leading to movement arrest was further inspected using both post-mortem MRI-scan and immunohistochemistry (Fig. 5A–C). The PPN is located in the caudal mesencephalon both rostro-dorsally, and ventrally to the decussation of the white matter track coming from the paired superior cerebellar peduncle, which goes towards

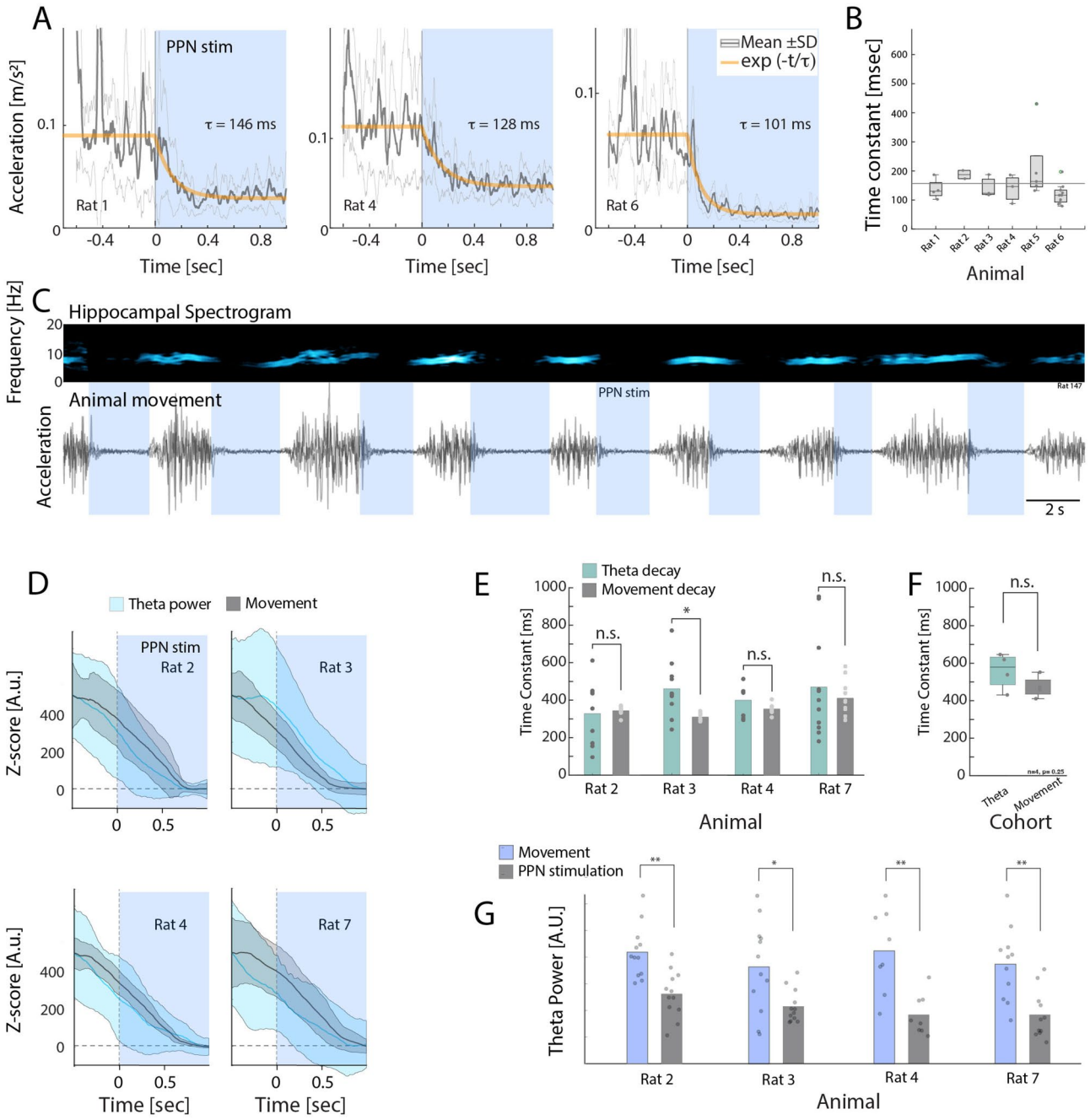

Fig. 4. Decay dynamics of movement and theta rhythm following PPN stimulation are similar. (**A**) The mean movement before and during PPN stimulation (accelerometer measurement ± standard deviation, SD, as the grey lines) for three sample animals. An exponential decay was fitted to the mean (orange line). (**B**) Whisker plot of time constants of the exponential decay fit for individual instances and animals. The mean time constant was 157 ms across animals. (**C**) A sample trial of hippocampal LFP spectral content (top) during movement and evoked arrest (blue regions), which was measured by accelerometry (bottom). (**D**) Mean ± SD for the hippocampal theta power (cyan) and accelerometry (grey) for four sample animals before and after the onset of PPN stimulation (blue region). (**E**) Histogram of time constants of decay of the theta rhythm (cyan) and movement (grey) across animals. There was no significant difference (n.s.) in the mean of time constants for theta rhythm vs. movement in 3 out of 4 animals. (**F**) Comparison of the mean of the time constants over the cohort shows no significant difference. (**G**) The integrated theta power in the hippocampal LFP during movement compared with during PPN stimulation in each animal. All show signifcant decrease in power. Wilcoxon signed-rank test, ∗ $p<0.05$, ∗∗ $p<0.01$.

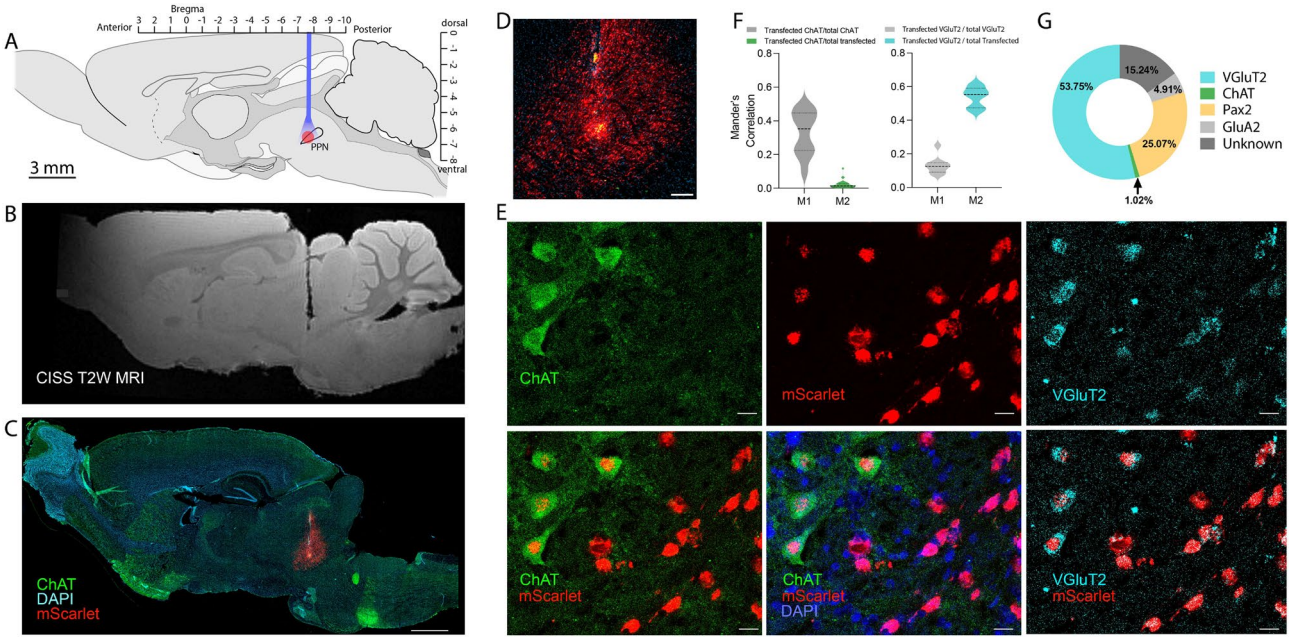

Fig. 5. The transfected cells in PPN. (**A**) The injection of virus and implantation of optical fiber in sagittal stereotaxic coordinates. (**B**) Post-mortem reconstruction of the location of the optical fiber (MRI-structural scan, track shown in black). (**C**) histological section of the same tissue as in (**B**) with the viral reporter (mScarlet using immunohistochemistry) in red, Cholinergic cells (ChAT) in green, and nuclei (DAPI) in blue (scale bar = 1000 μm, cerebellum missing). (**D**) Zoomed-in view of the injection site in (**C**) shows mScarlet reporter in red (detected using RNAscope) and ChAT cells in green (scale bar = 200 μm). (**E**) Among the transfected cells were cholinergic cells (ChAT immunohistochemistry, upper and lower left, and middle) and glutamatergic (VGluT2, upper and lower right, in cyan using RNAscope). DAPI was used as a nuclear stain (shown in blue,scale bar = 20 μm). (**F**) Colocalization was quantified using Manders correlation of a fraction of ChAT (left) overlapping with mScarlet out of all ChAT (M1) and all transfected (M2) and glutamatergic cells (right) overlapping with mScarlet out of all glutamatergic cells (M1) and all transfected cells (M2). (**G**) Manual counting of colocalization of VGluT2, ChAT, and GluA2 out of all infected cells in percent. N = 3 rat brains, n = 9–10 sections. Illustrations in (**A**) were adapted with permission from[51].

the thalamus. This white matter track is seen as a slightly darker shadow found at the tip of the vestige from the optical fiber in the structural magnetic resonance imaging (MRI) scan (Fig. 5B). The same tissue was sliced and stained using immunohistochemistry and imaged using fluorescent microscopy (Fig. 5C). This revealed the area of transfection, where the viral reporter (mScarlet) appears red. Since the PPN is the only nucleus in the area that contains cholinergic neurons, the staining of cholinergic neurons (ChAT antibody in green) ensures the appropriate location of the fiber and virus (Supplementary Fig. 4). The cholinergic neurons were few in number, sparsely scattered, and difficult to see, although somata were identified (Fig. 5D,E). To get a better grasp of the location of the part of the PPN that induces movement arrest, some of the brains were cleared and imaged using light sheet microscopy where the rostral location of the virus injection and optical fiber location are visible concerning the cholinergic somata (ChAT staining, Supplementary movie 2). The location of the successful injection was in the rostral aspects of the PPN nucleus in agreement with previous observations[7]. Next, we investigated what cell types in PPN were transfected and potentially responsible for the behavioral phenotype. Besides cholinergic neurons, the PPN also consists of glutamatergic and GABAergic neurons[18,24,52]. The transfected cells were identified using a combination of immunohistochemistry and RNAscope. The transfected cells were primarily glutamatergic, i.e. colocalization of red (mScarlet) and glutamatergic marker (VGluT2, the vesicle glutamate transporter type 2, Fig. 5E). A staining was also performed to identify cells with glutamate receptors (GluA2-subunit). The fractions were quantified using Menders correlation (Fig. 5F) and manual counting (Fig. 5G). There were only a few cholinergic neurons, but out of these, many also colocalized with VGluT2 (Supplementary Fig. 5). Such dual neuronal identity has been reported previously[52,53]. The low number of transfected cholinergic neurons is likely due to the generally low number of cholinergic neurons in the anterior end[53], which was the target of our investigation. There were also PAX2-positive among the infected and, therefore, likely GABAergic neurons, but the fraction was smaller than that of Glutamatergic (25% vs. 54%). The observation that the majority of infected cells were glutamatergic, combined with the induction of movement arrest, is in agreement with the observation from mice, where a subset of glutamatergic neurons, which express the gene Chx10, can induce similar movement arrest[4]. It is still unknown whether glutamatergic cells that do not contain the Chx10 gene can also cause motor arrest.

Discussion

For the brain to perceive events, the location in space has to be matched with the time of a given event[36,37]. The hippocampal formation has a key role in linking the "where" and the "when" during spatial navigation, and this is associated with a prominent electrical activity, the theta rhythm. The body's movement and the commands to contract muscles must be accounted for in the hippocampal formation. Although regions of the brainstem have been known to suppress motor reflexes[54] and arrest movement[16,55], the recent observation that the PPN and CnF can induce a global arrest of movement[4,7,13] introduces a new means to tamper with the link between movement and cognition internally. It is unknown how this lower-level nucleus can affect the movement-associated brain rhythm at the hippocampal level in this motor hierarchy. In this report, we tested the impact of PPN-induced movement arrest on the ongoing hippocampal theta rhythm. Specifically, we tested three hypotheses of what to expect following internally generated motor arrest and the effect on hippocampal activity (Fig. 1).

The PPN was optogenetically activated to induce movement arrest. The hippocampal theta rhythm was simultaneously recorded and the movement was assessed with accelerometry (Figs. 2, 3, 4) and videography (Supplementary Movie 1). The animal was either roaming around or on a treadmill. During the movement, there was a distinct rhythmic electrical activity in the hippocampus at 6–9 Hz, the theta rhythm. Upon activation of the PPN, this theta rhythm swiftly vanished and the movement was halted. In the attempt to establish a causal order between the halt of execution of movement and the obstruction of theta rhythm, the time constants of these two events were estimated. The decay time of both processes was on the order of 2–300 ms and not distinguishable given our experimental conditions. Hence, we cannot infer a causal relationship, only an association.

How can activation of a low-level brainstem nucleus obstruct the cortical rhythms? The PPN has a subpopulation of cholinergic neurons, which is part of the cholinergic arousal system. The PPN and the arousal system are well-known to desynchronize neocortical activity[39] and may also be implicated in postural disorders in Parkinson's disease[56]. Although the cells responsible for the movement arrest are not cholinergic[4,19], there were indeed cholinergic neurons among the infected cells (Fig. 5). In fact, almost all the identified cholinergic neurons in the fiber tip vicinity also express glutamatergic neurotransmitters (VGluT2, Supplementary Fig. 5). Co-expression of ChAT and VGluT2 has been observed in other investigations, although to a smaller extent[52,57,58]. Besides glutamatergic and cholinergic cells, a fraction of gabaergic neurons (PAX2, 25%) were also transfected. The effects of the optogenetic activation of these are unknown. We primarily aim for the rostral part of PPN that has fewer cholinergic neurons compared with the caudal end of the PPN[53]. Previous investigations have indicated that the frequency of stimulation is important[34] and the gamma range (40–60 Hz) tends to have a stronger activation than other frequencies due to the intrinsic membrane properties[59]. Nevertheless, activating ascending Cholinergic fibers induces a strong hippocampal theta rhythm, rather than blocking it[39,60]. For instance, activation of PPN using infused carbachol and electrical stimulation induces hippocampal theta in rats[40,41]. During sleep and drowsiness, we observed evoked theta rhythm following PPN stimulation (Supplementary Fig. 6), consistent with the previous observation of cholinergic facilitation effect on hippocampal theta rhythm. Besides being present under different contingencies, the type 2 theta rhythm is slightly lower in frequency than the type 1 (Supplementary Fig. 6F,G). Hence, the input of ascending fibers from PPN to the hippocampus cannot explain the obstruction of the theta rhythm associated with the arrest of movement. This indicates that the effect on theta rhythm is likely linked to immobility, hence supporting the alternative hypothesis 1 (Fig. 1B).

In conclusion, our results demonstrate that the motor arrest induced internally by stimulation of PPN also obstructs the ongoing hippocampal theta rhythm (type 1). Further, there was no fear-related induction of type-2 theta rhythm in the hippocampus following the motor arrest. If the induced arrest of movement was akin to behavioral freeze, the brain should be alert, and be accompanied by a type 2 theta rhythm in the hippocampus. For these reasons, we suggest that the part of the PPN that can induce movement arrest represents the motor part of an omnipotent arrest of movement.

Materials and methods

Animals and ethical statement

Wild-type Long Evans adult male rats (aged 12–24 weeks, 450–600 g) were used to perform the experiments. The rats were obtained from Charles River Laboratories and housed in cages equipped with bedding, food, water, temperature, and air sensors and kept in a 12 h light/ 12 h dark cycle. Before any surgical procedure, the rats were housed in pairs for one week in the animal housing facility for acclimatization. All the experimental procedures complied with ARRIVE guidelines and the Council of the European Union (86/609/EEC). The study was approved by the Danish Veterinary and Food Administration (animal research permission number 2019-15-0201-00018).

Surgery, virus injection, fiber implantation and optogenetics

All the surgical procedures on Wild-type adult rats were performed in aseptic conditions. The rats were anesthetized using gas anesthesia (isoflurane in a mixture of air and oxygen). The surgery room was divided into 2 sections: a dirty and a clean section. In the dirty section, an initial part of the procedure was performed such as shaving hair off the rat's surgical area and cleaning the shaved area with chlorhexidine (from inside to outside) followed by cleaning with ethanol (70%). Later, the rat was moved to the clean section, which is the surgery table with a stereotaxic robot, on a heating pad with a temperature sensor, and an oximeter was used to monitor the oxygen level during the surgery. The head of the rat was fixed using the ear bars. Ocryl gel was used to keep the eyes moist and the surgical area was again cleaned with 70% ethanol. Then a sterile drape was placed on the anesthetized rat and a hole was made on the drape at the surgical area of interest and Mepitel film with a fine cut in the middle (Molnlycke Healthcare, Goteborg, Sweden) was placed on the shaved sterile area of the rat.

An incision was made on the skin and bulldog forceps were used to stretch the skin and increase the visibility of the skull. The skull was made completely dry using electrocautery and hydrogen peroxide. The skull was

painted with a thin layer of dental cement (C&B Metabond quick adhesive cement system, Parkell). A 3D-printed head plate with an attached copper mesh[61] was glued on the skull, craniotomy was performed and an AAV virus (AAV9-CamKIIa-ChrimsonR-mScarlet-Kv2.1, which was a gift from Christopher Harvey via Addgene.org by Ref.[62]) was injected with a glass capillary using a stereotaxic robot (Neurostar GmbH, Tubingen, Germany) into the PPN (500 nl injection volume, Fig. 1A, coordinates (DV: 7.8, ML: 1.58, AP: -7.8). An optical fiber (ø200 μ m, 10 mm length, CFML12L10, Thorlabs, Sweden) was subsequently implanted 200 µm above the injection site and the hole was closed using cyanoacrylate glue followed by dental cement. A copper crown was built out of the mesh using a thin layer of dental cement to protect the protruding optical fiber ferrule[61]. The crown also served as a Faraday cage during electrical recordings. The post-operative care was given where the rats were given buprenorphine mixed with Nutella[63] (sublingual tablets 0.2 mg crushed to powder and mixed with 1 g Nutella, dose = 0.4 mg/kg, every 12 h for 3 days) and carprofen (subcutaneously (s.c.), 5 mg/kg, once a day for 5 days) as analgesic and anti-inflammatory and Baytril (s.c., 5 mg/kg, once/day for 10 days) as antibiotic drugs. The rat was monitored twice/day for 3 consecutive days followed by once/day for 7 days. Optogenetic stimulation was performed using a red LED laser (625 nm, M625F2, Thorlabs, Sweden) attached to a patch cable and a connecting sleve on the animal implant. The stimulation was either constant light or pulses of 100 Hz with a 50% duty cycle. The power was adjusted to elicit appropriate response, although a maximum of 13 mW power output from the LED.

Measurement of theta rhythm: implantation of electrocorticographic electrodes

3–4 weeks after the injection of the AAV virus, the virus shows expression. Therefore, after 4 weeks the implant was tested for whether it could induce movement arrest when using an optogenetic pulse train delivered to PPN with a red LED laser (625 nm, Model M625F2, Thorlabs, Inc.). After confirming the motor arrest, a second surgery was performed where 4 tungsten electrodes were implanted in the primary motor cortex (AP = 1.56–2.52, ML =2.2–2.3 and DV = 2.0–2.3) and 4 in the hippocampus (AP = -3.3–3.6, ML = 2.0 and DV = 3.0–3.4) together with 1 reference silver and 1 ground silver electrodes. Post-surgical care was given as reported by Ref.[64].

The Teflon-coated tungsten or silver wires were inserted into the hippocampal formation in the CA1-CA3 where the local field potential is strongest[65,66]. The electrical signals were recorded using a miniaturized head stage with integrated accelerometers tethered with a lightweight interface cable to the amplifier (RHD 32 channel head stage, Intan technologies). The movement was measured using accelerometers available on the head stage. The reading, which was in Volt was converted to acceleration as 340 mV/g, where 1 g is 1 m/s^2.

RNAscope

At the end of the experiment, the rats were perfused with 4% formaldehyde. The perfusion procedure was adapted from previous studies[63]. The brains were extracted and fixed again using formaldehyde for 4 h followed by cryoprotection using 30% (w/v) sucrose for 48 h. Later the brains were stored at − 80 °C. 20 µm thin brain sections were collected on Superfrost plus glass slides (Thermo Fisher Scientific GmbH, Germany) and stored at − 20 °C until further use. In situ labeling of targeted mRNA was done by RNAscope method, using a commercially available kit (Advanced Cell Diagnostics, Hayward, CA) according to the manufacturer's protocol. Dehydrated tissue sections were blocked with hydrogen peroxide and boiled in target retrieval reagent for 5 min. Then the tissue was incubated with protease plus for 30 min at 40 °C and targeted probes against mScarlet (Cat No. 572421) and VGluT2 (Cat No. 319171-C3) (Advanced Cell Diagnostics, Hayward, CA) were hybridized on the tissue for 2 h in Hybez oven (Advanced Cell Diagnostics, Hayward, CA) followed by a series of signal amplification and washing steps. The signal was visualized by incubation slides with OpalTM570 and OpalTM690 reagents (1:1000) (Perkin Elmer). Then sections were processed for immunohistochemistry.

Immunohistochemistry

After completing the RNAscope procedure, the same brain sections were used to perform immunohistochemistry. This procedure was adapted from prior studies[67,68]. The slides with brain sections were washed in 1X phosphate-buffered saline (PBS) followed by incubated them with Blocking solution (5% bovine serum albumin, 5% fetal bovineserum, 0.3% Triton X-100, 1% PBS) for 2 hours at room temperature followed by administration of primary antibodies such as ChAT (goat polyclonal, 1:500, EMD Millipore AB144P), Pax2 (rabbit polyclonal, 1:500 dilution, Invitrogen UD283859) and GluA2 (mouse monoclonal, 1:200 dilution, EMD Millipore MAB397) for overnight at 4°C. The next day, the slices were washed and incubated with the following secondary antibodies (1:500): donkey anti-goat Alexa Fluor 647 (Abcam, AB150135), donkey anti-rabbit Alexa Fluor 647 (Invitrogen, A31573), donkey anti-rabbit Alexa Fluor 488 (Invitrogen, A11055), donkey anti-mouse Alexa Fluor 647 (Invitrogen, A31571) and 4',6-diamidino-2-phenylindole (DAPI, 1:1000; Sigma-Aldrich) at room temperature for 2 h. DAKO mounting medium was used to mount the slides followed by visualizing under Axio scan Z1 and confocal microscope using 20X magnification. The images captured by microscopes were analyzed using Zen Lite 3.1 and ImageJ software. The correlation coefficient was computed by using the Manders correlation coefficient and metric matrix[69]. Adobe Illustrator was used to create a contour of the brain section/s to show the viral injection site (Fig. 1A, Supplementary Figs. 2–5). Graph-pad prism was used to create graphs.

Tissue clearing and light sheet microscopy

To view the viral expression in 3D one rat brain was cut in half and cleared using a 2nd generation ethyl-cinnamate clearing method (2ECi clearing, Supplementary Movie 2)[70] and the other brain was cut from the sides sagittally and cleared using Adipo-clear method (Supplementary Movie 2)[71]. During the 2ECi procedure, the brain was stained with a nucleic acid stain (Sytox, green nucleic acid stain, 1:5000, ThermoFisher Scientific, cat. S7020). The brain was imaged on an LCS Spim light-sheet microscope (Bruker). The endogenous fluorescent reporter (mScarlet[72]) was visible as a red fluorophore (Supplementary Movie 2) During the Adipo-clear procedure, the

brain was stained with primary antibodies, ChAT (goat polyclonal, 1:400, EMD Millipore AB144P) and RFP (rabbit, 1:1000, Rockland) followed by incubation with secondary antibodies, donkey anti-goat (1:500, Alexa fluor 647) and donkey anti-rabbit (1:500, Alexa fluor 555). The cleared brain was imaged with a Zeiss LS7 microscope (Supplementary Movie 2).

Magnetic resonance imaging

Structural Magnetic resonance imaging (MRI) was done for post-mortem anatomical reconstruction and verification of electrode and optical fiber location. After transcardial perfusion using PBS followed by paraformaldehyde (PFA, 4%) the tissue was kept overnight in PFA followed by transferring to sucrose solution (30% w/v) and finally to PBS. Later the brain was transferred to a tube containing fluorinert (FC-40, Sigma-Aldrich) to reduce the background signal. The tube was placed in a 9.4 T pre-clinical MRI scanner (BioSpec 94/30; Bruker Biospin, Ettlingen, Germany) equipped with a 1.5 T/m gradient coil. A T2-weighted scan sequence was performed, the Constructive Interference in Steady State (CISS) in isotropic resolution of 50 um (Fig. 4B and Supplementary Movie 2).

Data analysis

The LFP potential recordings from the hippocampus were filtered using custom-designed Matlab code (Mathworks 2020b) consisting of a 3-pole Butterworth filter. The spectrogram was calculated using the multi-taper method described in the previous report[66]. Sliding temporal windows of $T = 1.6\,\mathrm{s}$ were used to estimate the spectrogram with a 90% sliding overlap and with discrete jumps of 10% of the size of the window, i.e., 160 ms. The spectra were estimated as an average over independent estimates using the first two tapers of the discrete prolate spherical sequences[73] before performing a Fourier transform (functions *fft.m* and *dpss.m* in Matlab). To estimate the decay theta spectral content, a smaller temporal window of $T = 1.0\,\mathrm{s}$ was used. The time constant for the decay in the movement was estimated from the full-wave rectified accelerometer measurement, which was averaged across x, y, and z directions and smoothed. The decay was fitted to an exponential decay model, $\exp(-t/\tau)$, where τ presents the decay time constant.

Data availability

The data that support the findings of this study are available from the corresponding author, RWB, upon reasonable request.

Received: 1 February 2025; Accepted: 7 May 2025
Published online: 23 May 2025

References

1. Roseberry, T. et al. Cell-type-specific control of brainstem locomotor circuits by basal ganglia. *Cell* **164**, 526–537. https://doi.org/10.1016/j.cell.2015.12.037 (2016).
2. Wessel, J. R. & Aron, A. R. On the globality of motor suppression: Unexpected events and their influence on behavior and cognition. *Neuron* **93**, 259–280. https://doi.org/10.1016/j.neuron.2016.12.013 (2017).
3. Roelofs, K. Freeze for action: Neurobiological mechanisms in animal and human freezing. *Philos. Trans. R. Soc. B Biol. Sci.* **372**, 20160206. https://doi.org/10.1098/rstb.2016.0206 (2017).
4. Goñi-Erro, H., Selvan, R., Caggiano, V., Leiras, R. & Kiehn, O. Pedunculopontine chx10+ neurons control global motor arrest in mice. *Nat. Neurosci.* **26**, 1516–1528. https://doi.org/10.1038/s41593-023-01396-3 (2023).
5. Josset, N. et al. Distinct contributions of mesencephalic locomotor region nuclei to locomotor control in the freely behaving mouse. *Curr. Biol.* **28**, 884–901. https://doi.org/10.1016/j.cub.2018.02.007 (2018).
6. Dautan, D. et al. Modulation of motor behavior by the mesencephalic locomotor region. *Cell Rep.* **36**, 109594. https://doi.org/10.1016/j.celrep.2021.109594 (2021).
7. Carvalho, M. M. et al. A brainstem locomotor circuit drives the activity of speed cells in the medial entorhinal cortex. *Cell Rep.* **32**, 108123. https://doi.org/10.1016/j.celrep.2020.108123 (2020).
8. Takakusaki, K., Habaguchi, T., Ohtinata-Sugimoto, J., Saitoh, K. & Sakamoto, T. Basal ganglia efferents to the brainstem centers controlling postural muscle tone and locomotion: A new concept for understanding motor disorders in basal ganglia dysfunction. *Neuroscience* **119**, 293–308. https://doi.org/10.1016/S0306-4522(03)00095-2 (2003).
9. Takakusaki, K., Chiba, R., Nozu, T. & Okumura, T. Brainstem control of locomotion and muscle tone with special reference to the role of the mesopontine tegmentum and medullary reticulospinal systems. *J. Neural Transm.* **123**, 695–729. https://doi.org/10.1007/s00702-015-1475-4 (2016).
10. Shik, M. L., Severin, F. V. & Orlovskii, G. N. Control of walking and running by means of electrical stimulation of the midbrain. *Biofizica* **11**, 659–666 (1966).
11. Caggiano, V. et al. Midbrain circuits that set locomotor speed and gait selection. *Nature* **553**, 455–460. https://doi.org/10.1038/nature25448 (2018).
12. Carbo-Tano, M. et al. The mesencephalic locomotor region recruits v2a reticulospinal neurons to drive forward locomotion in larval zebrafish. *Nat. Neurosci.* **26**, 1775–1790. https://doi.org/10.1038/s41593-023-01418-0 (2023).
13. Tello, A. J. et al. Dopamine-sensitive neurons in the mesencephalic locomotor region control locomotion initiation, stop, and turns. *Cell Rep.* **43**, 114187. https://doi.org/10.1016/j.celrep.2024.114187 (2024).
14. Lindén, H., Petersen, P. C., Vestergaard, M. & Berg, R. W. Movement is governed by rotational neural dynamics in spinal motor networks. *Nature* **610**, 526–531. https://doi.org/10.1038/s41586-022-05293-w (2022).
15. Berg, R. W., Willumsen, A. & Lindén, H. When networks walk a fine line: Balance of excitation and inhibition in spinal motor circuits. *Curr. Opin. Physiol.* **8**, 76–83. https://doi.org/10.1016/j.cophys.2019.01.006 (2019).
16. Capelli, P., Pivetta, C., Esposito, M. S. & Arber, S. Locomotor speed control circuits in the caudal brainstem. *Nature* **551**, 373–377. https://doi.org/10.1038/nature24064 (2017).
17. Noga, B. R. & Whelan, P. J. The mesencephalic locomotor region: Beyond locomotor control. *Front. Neural Circuits* **16**, 785. https://doi.org/10.3389/fncir.2022.884785 (2022).
18. Ryczko, D. The mesencephalic locomotor region: Multiple cell types, multiple behavioral roles, and multiple implications for disease. *Neuroscientist* **30**, 347–366. https://doi.org/10.1177/10738584221139136 (2024).

19. Leiras, R., Cregg, J. M. & Kiehn, O. Brainstem circuits for locomotion. *Annu. Rev. Neurosci.* **45**, 63–85. https://doi.org/10.1146/annurev-neuro-082321-025137 (2022).
20. Goetz, L. et al. On the role of the pedunculopontine nucleus and mesencephalic reticular formation in locomotion in nonhuman primates. *J. Neurosci.* **36**, 4917–4929. https://doi.org/10.1523/JNEUROSCI.2514-15.2016 (2016).
21. Mori, S., Nishimura, H., Kurakami, C., Yamamura, T. & Aoki, M. Controlled locomotion in the mesencephalic cat: Distribution of facilitatory and inhibitory regions within pontine tegmentum. *J. Neurophysiol.* **41**, 1580–1591. https://doi.org/10.1152/jn.1978.41.6.1580 (1978).
22. Skinner, R. & Garcia-Rill, E. The mesencephalic locomotor region (mlr) in the rat. *Brain Res.* **323**, 385–389. https://doi.org/10.1016/0006-8993(84)90319-6 (1984).
23. Chang, S. J. et al. Deep brain stimulation of midbrain locomotor circuits in the freely moving pig. *Brain Stimul.* **14**, 467–476. https://doi.org/10.1016/j.brs.2021.02.017 (2021).
24. Mena-Segovia, J. & Bolam, J. P. Rethinking the pedunculopontine nucleus: From cellular organization to function. *Neuron* **94**, 7–18. https://doi.org/10.1016/j.neuron.2017.02.027 (2017).
25. Ferreira-Pinto, M. J. et al. Functional diversity for body actions in the mesencephalic locomotor region. *Cell* **184**, 4564–4578. https://doi.org/10.1016/j.cell.2021.07.002 (2021).
26. Ferreira-Pinto, M. J., Ruder, L., Capelli, P. & Arber, S. Connecting circuits for supraspinal control of locomotion. *Neuron* **100**, 361–374. https://doi.org/10.1016/j.neuron.2018.09.015 (2018).
27. Koba, S. et al. A brainstem monosynaptic excitatory pathway that drives locomotor activities and sympathetic cardiovascular responses. *Nat. Commun.* **13**, 5079. https://doi.org/10.1038/s41467-022-32823-x (2022).
28. Botta, P. et al. An amygdala circuit mediates experience-dependent momentary arrests during exploration. *Cell* **183**, 605–619. https://doi.org/10.1016/j.cell.2020.09.023 (2020).
29. Roseberry, T. K., Lalive, A. L., Margolin, B. D. & Kreitzer, A. C. *Locomotor Suppression by a Monosynaptic Amygdala to Brainstem Circuit* (2019).
30. Woolf, N. J. & Butcher, L. L. Cholinergic systems in the rat brain: III. Projections from the pontomesencephalic tegmentum to the thalamus, tectum, basal ganglia, and basal forebrain. *Brain Res. Bull.* **16**, 603–637. https://doi.org/10.1016/0361-9230(86)90134-6 (1986).
31. Xiao, C. et al. Cholinergic mesopontine signals govern locomotion and reward through dissociable midbrain pathways. *Neuron* **90**, 333–347. https://doi.org/10.1016/j.neuron.2016.03.028 (2016).
32. French, I. T. & Muthusamy, K. A. A review of the pedunculopontine nucleus in parkinson's disease. *Front. Aging Neurosci.* **10**, 99. https://doi.org/10.3389/fnagi.2018.00099 (2018).
33. Mirelman, A. et al. Gait impairments in parkinson's disease. *Lancet Neurol.* **18**, 697–708. https://doi.org/10.1016/S1474-4422(19)30044-4 (2019).
34. Virmani, T., Urbano, F. J., Bisagno, V. & Garcia-Rill, E. The pedunculopontine nucleus: From posture and locomotion to neuroepigenetics. *AIMS Neurosci.* **6**, 219–230. https://doi.org/10.3934/Neuroscience.2019.4.219 (2019).
35. Pahapill, P. A. The pedunculopontine nucleus and parkinson's disease. *Brain* **123**, 1767–1783. https://doi.org/10.1093/brain/123.9.1767 (2000).
36. Buzsáki, G. & Moser, E. I. Memory, navigation and theta rhythm in the hippocampal-entorhinal system. *Nat. Neurosci.* **16**, 130–138. https://doi.org/10.1038/nn.3304 (2013).
37. Joshi, A. et al. Dynamic synchronization between hippocampal representations and stepping. *Nature* **617**, 125–131. https://doi.org/10.1038/s41586-023-05928-6 (2023).
38. Lee, A. et al. Identification of a brainstem circuit regulating visual cortical state in parallel with locomotion. *Neuron* **83**, 455–466. https://doi.org/10.1016/j.neuron.2014.06.031 (2014).
39. Green, J. D. & Arduini, A. A. Hippocampal electrical activity in arousal. *J. Neurophysiol.* **17**, 533–557. https://doi.org/10.1152/jn.1954.17.6.533 (1954).
40. Kinney, G. G., Vogel, G. W. & Feng, P. Brainstem carbachol injections in the urethane anesthetized rat produce hippocampal theta rhythm and cortical desynchronization: A comparison of pedunculopontine tegmental versus nucleus pontis oralis injections. *Brain Res.* **809**, 307–313. https://doi.org/10.1016/S0006-8993(98)00878-6 (1998).
41. Vertes, R., Colom, L., Fortin, W. & Bland, B. Brainstem sites for the carbachol elicitation of the hippocampal theta rhythm in the rat. *Exp. Brain Res.* **96**, 110. https://doi.org/10.1007/BF00234110 (1993).
42. Buzsáki, G. Theta rhythm of navigation: Link between path integration and landmark navigation, episodic and semantic memory. *Hippocampus* **15**, 827–840. https://doi.org/10.1002/hipo.20113 (2005).
43. Bender, F. et al. Theta oscillations regulate the speed of locomotion via a hippocampus to lateral septum pathway. *Nat. Commun.* **6**, 8521. https://doi.org/10.1038/ncomms9521 (2015).
44. Ranck, J. B. Studies on single neurons in dorsal hippocampal formation and septum in unrestrained rats. *Exp. Neurol.* **41**, 462–531. https://doi.org/10.1016/0014-4886(73)90290-2 (1973).
45. Dunn, S., Town, S. M., Bizley, J. K. & Bendor, D. Behaviourally modulated hippocampal theta oscillations in the ferret persist during both locomotion and immobility. *Nat. Commun.* **13**, 5905. https://doi.org/10.1038/s41467-022-33507-2 (2022).
46. Kropff, E., Carmichael, J. E., Moser, E. I. & Moser, M.-B. Frequency of theta rhythm is controlled by acceleration, but not speed, in running rats. *Neuron* **109**, 1029–1039. https://doi.org/10.1016/j.neuron.2021.01.017 (2021).
47. Vanderwolf, C. Hippocampal electrical activity and voluntary movement in the rat. *Electroencephalogr. Clin. Neurophysiol.* **26**, 407–418. https://doi.org/10.1016/0013-4694(69)90092-3 (1969).
48. Foster, T. C., Castro, C. A. & McNaughton, B. L. Spatial selectivity of rat hippocampal neurons: Dependence on preparedness for movement. *Science* **244**, 1580–1582. https://doi.org/10.1126/science.2740902 (1989).
49. Tendler, A. & Wagner, S. Different types of theta rhythmicity are induced by social and fearful stimuli in a network associated with social memory. *ELife* **4**, 614. https://doi.org/10.7554/eLife.03614 (2015).
50. Silva, C., Young, C. K. & McNaughton, N. Prefrontal and hippocampal theta rhythm show anxiolytic-like changes during periaqueductal-elicited "panic" in rats. *Hippocampus* **32**, 679–694. https://doi.org/10.1002/hipo.23459 (2022).
51. Swanson, L. W. Brain maps 4.0-structure of the rat brain: An open access atlas with global nervous system nomenclature ontology and flatmaps. *J. Compar. Neurol.* **526**, 935–943. https://doi.org/10.1002/cne.24381 (2018).
52. Luquin, E., Huerta, I., Aymerich, M. S. & Mengual, E. Stereological estimates of glutamatergic, gabaergic, and cholinergic neurons in the pedunculopontine and laterodorsal tegmental nuclei in the rat. *Front. Neuroanat.* **12**, 34. https://doi.org/10.3389/fnana.2018.00034 (2018).
53. Mena-Segovia, J., Micklem, B., Nair-Roberts, R., Ungless, M. & Bolam, J. Gabaergic neuron distribution in the pedunculopontine nucleus defines functional subterritories. *J. Compar. Neurol.* **515**, 397–408. https://doi.org/10.1002/cne.22065 (2009).
54. Magoun, H. W. & Rhines, R. An inhibitory mechanism in the bulbar reticular formation. *J. Neurophysiol.* **9**, 165–171. https://doi.org/10.1152/jn.1946.9.3.165 (1946).
55. Bouvier, J. et al. Descending command neurons in the brainstem that halt locomotion. *Cell* **163**, 1191–1203. https://doi.org/10.1016/j.cell.2015.10.074 (2015).
56. Karachi, C. et al. Cholinergic mesencephalic neurons are involved in gait and postural disorders in parkinson disease. *J. Clin. Investig.* **120**, 2745–2754. https://doi.org/10.1172/JCI42642 (2010).
57. Nasirova, N. et al. Dual recombinase fate mapping reveals a transient cholinergic phenotype in multiple populations of developing glutamatergic neurons. *J. Compar. Neurol.* **528**, 283–307. https://doi.org/10.1002/cne.24753 (2020).

58. Steinkellner, T., Yoo, J. H. & Hnasko, T. S. Differential expression of vglut2 in mouse mesopontine cholinergic neurons. *Eneuro* **6**, 2019. https://doi.org/10.1523/ENEURO.0161-19.2019 (2019).
59. Garcia-Rill, E. et al. Gamma band activity in the ras-intracellular mechanisms. *Exp. Brain Res.* **232**, 1509–1522. https://doi.org/10.1007/s00221-013-3794-8 (2014).
60. Vertes, R. P. An analysis of ascending brain stem systems involved in hippocampal synchronization and desynchronization. *J. Neurophysiol.* **46**, 1140–1159. https://doi.org/10.1152/jn.1981.46.5.1140 (1981).
61. Voroslakos, M. et al. 3d-printed recoverable microdrive and base plate system for rodent electrophysiology. *Bio-Protocol* **11**, 4137. https://doi.org/10.21769/BioProtoc.4137 (2021).
62. Chettih, S. N. & Harvey, C. D. Single-neuron perturbations reveal feature-specific competition in v1. *Nature* **567**, 334–340. https://doi.org/10.1038/s41586-019-0997-6 (2019).
63. Kaur, J. & Berg, R. W. Viral strategies for targeting spinal neuronal subtypes in adult wild-type rodents. *Sci. Rep.* **12**, 8627. https://doi.org/10.1038/s41598-022-12535-4 (2022).
64. Kaur, J. & Conti, E. Dataset on inflammation induced after lumbar puncture. *Data Brief* **34**, 106729. https://doi.org/10.1016/j.dib.2021.106729 (2021).
65. Buzsáki, G. Theta oscillations in the hippocampus. *Neuron* **33**, 325–340. https://doi.org/10.1016/S0896-6273(02)00586-X (2002).
66. Berg, R. W., Whitmer, D. & Kleinfeld, D. Exploratory whisking by rat is not phase locked to the hippocampal theta rhythm. *J. Neurosci.* **26**, 6518–6522. https://doi.org/10.1523/JNEUROSCI.0190-06.2006 (2006).
67. Meneghetti, M. et al. Soft monolithic infrared neural interface for simultaneous neurostimulation and electrophysiology. *Light Sci. Appl.* **12**, 127. https://doi.org/10.1038/s41377-023-01164-9 (2023).
68. Kaur, J., Mazzone, G. L., Aquino, J. B. & Nistri, A. Nicotine neurotoxicity involves low wnt1 signaling in spinal locomotor networks of the postnatal rodent spinal cord. *Int. J. Mol. Sci.* **22**, 572. https://doi.org/10.3390/ijms22179572 (2021).
69. Manders, E. M. M., Verbeek, F. J. & Aten, J. A. Measurement of co-localization of objects in dual-colour confocal images. *J. Microsc.* **169**, 1. https://doi.org/10.1111/j.1365-2818.1993.tb03313.x (1993).
70. Masselink, W. et al. Broad applicability of a streamlined ethyl cinnamate-based clearing procedure. *Development* **1**, 884. https://doi.org/10.1242/dev.166884 (2019).
71. Leong, I. New tissue processing technique for adipose tissues. *Nat. Rev. Endocrinol.* **14**, 128. https://doi.org/10.1038/nrendo.2018.8 (2018).
72. Bindels, D. S. et al. mscarlet: A bright monomeric red fluorescent protein for cellular imaging. *Nat. Methods* **14**, 53–56. https://doi.org/10.1038/nmeth.4074 (2017).
73. Percival, D. & Walden, A. *Spectral Analysis for Physical Applications—Multitaper and Conventional Univariate Techniques* (Cambridge University Press, 1998).

Acknowledgements

This work was supported by The Independent research fund Denmark, and the Carlsberg foundation. Thanks to Yuki Mori from Center for translational medicine for performing the MRI scans. Thanks to Palle Koch and Jakob F. Sørensen for help designing and constructing the treadmill. Funding: Lundbeck foundation (no: R366-2021-233) and Independent research fund Denmark (no. 8020-00436B).

Author contributions

R.W.B. and J.K. conceived and designed the experiments. J.K. performed the surgeries and data analysis of post-mortem tissue. J.K., R.W.B. performed the experiments. J.K. and M.B. performed immunohistochemistry. O.D. performed RNAscope. J.K. and G.H. performed tissue clearing. R.W.B. and S.K. analyzed the electrophysiology data. R.W.B. wrote the manuscript.

Declarations

Competing interests

The authors declare no competing interests.

Declaration of AI Assistance in writing

Artificial intelligence (AI) in the form of generative Large Language Models (ChatGPT-4) assisted in writing this manuscript. The use of ChatGPT was done by rewriting a section for improving clarity. The output was reviewed and edited and adapted for meaning. All authors have read the manuscript and take full responsibility of the content.

Additional information

Supplementary Information The online version contains supplementary material available at https://doi.org/10.1038/s41598-025-01695-8.

Correspondence and requests for materials should be addressed to R.W.B.